Journal of Computational Physics **174,** 306–326 (2001)
doi:10.1006/jcph.2001.6912, available online at http://www.idealibrary.com on IDEAL®

# Stability Analysis for Different Formulations of the Nonlinear Term in $P_N - P_{N-2}$ Spectral Element Discretizations of the Navier–Stokes Equations

D. Wilhelm and L. Kleiser

*Institute of Fluid Dynamics, Eidgenössische Technische Hochschule (ETH) Zürich, ETH Zentrum, CH-8092 Zürich, Switzerland*
E-mail: dirk@ifd.mavt.ethz.ch and kleiser@ifd.mavt.ethz.ch

Received January 11, 2000; revised July 19, 2001

We show that for the $P_N - P_{N-2}$ spectral element method, in which velocity and pressure are approximated by polynomials of order $N$ and $N-2$, respectively, numerical instabilities can occur in the spatially discretized Navier–Stokes equations. Both a staggered and nonstaggered arrangement of the $N-2$ pressure points are considered. These instabilities can be masked by viscous damping at low Reynolds numbers. We demonstrate that the instabilities depend on the formulation of the nonlinear term. The numerical discretization is stable for the convective form but unstable for the divergence and the skew-symmetric form. Further numerical analysis indicates that this instability is not caused by nonlinear effects, since it occurs for linearized systems as well. An eigenvalue analysis of the fully discretized system shows that an instability is introduced by the formulation of the nonlinear term. We demonstrate that the instability is related to the divergence error of the computed solution at those velocity points at which the continuity equation is not enforced. 

*Key Words:* spectral element method; Navier–Stokes equations; numerical instability; incompressible flow; formulation of nonlinear term.

## 1. INTRODUCTION

We consider flow simulations at high Reynolds numbers with a scheme that provides high accuracy and geometrical flexibility. For this purpose, the incompressible Navier–Stokes equations are discretized in time by mixed implicit/explicit finite-difference schemes and in space by a spectral element method (SEM). Spectral element methods are based on the decomposition of the computational domain into a number $K$ of subdomains. In each subdomain the solution is expanded in tensor-product-based Jacobi polynomials of order



0021-9991/01 $35.00

$N$. As basis functions, Lagrange polynomials based on Gauss and Gauss–Lobatto points are often used.

In numerical simulations of incompressible flows the momentum equations have to be solved under the continuity constraint. This can be achieved either by solving the entire system for pressure and velocity in a coupled manner or by decoupling the velocity from the pressure. In spectral element simulations both approaches have been employed. For example, Karniadakis and co-workers [14, 15, 24] use a high-order splitting method, where velocity and pressure are discretized at the same points ($P_N - P_N$ method). They deduce a Poisson equation for the pressure, which is solved at every time step together with boundary conditions derived from the previous velocity fields. The method introduces a splitting error, which can be made of higher order in the time step. To avoid this splitting error, the influence matrix technique (see, e.g., [4, 16, 17]) can be applied, which is also a $P_N - P_N$ method. This technique also utilizes a Poisson equation for the pressure, but the boundary conditions are derived from the continuity equation at the boundaries of the domain. This provides a clean treatment of the pressure boundary conditions but has a drawback of high computational costs when in three dimensions (3D) no homogeneity can be exploited in any direction. However, if the computational domain is periodic in one or two directions, the influence matrix technique can be applied very efficiently (see, e.g., [10, 11]).

When momentum and continuity equations are solved in a coupled fashion, the spaces of the basis functions for the velocity $\underline{u}$ and the pressure $q$ have to satisfy the well-known *inf-sup* condition (see, e.g., [3]). To comply with this condition in SEM, the pressure $q$ and the velocity $\underline{u}$ are often approximated by functions belonging to different spaces. For example, in the $P_N - P_{N-2}$ method, $\underline{u}$ is represented by polynomials two orders higher than $q$ [7, 8, 19]. By this approach, pressure boundary conditions are avoided, and the entire system can be solved using the Uzawa technique [3]. In the present paper, we analyze two variants of the $P_N - P_{N-2}$ SEM. One is the classical method of Maday and Patera [19], where $\underline{u}$ is discretized at the Gauss–Lobatto–Legendre (GL) points and $q$ at the Gauss–Legendre (G) points. The other one is the $P_N - P_{N-2}$ method used by Rønquist [22] in which the velocity $\underline{u}$ is discretized at the $N + 1$ GL points and the pressure at the $N - 1$ inner GL points in each element. The first method is referred as the "staggered" approach and the second as the "nonstaggered" approach throughout this paper.

The discretization of the incompressible Navier–Stokes equations can be performed in several ways, which differ in the formulation of the nonlinear term (for an overview of the formulations see, e.g., Gresho [9]). Among these alternatives are the convective form $(\underline{u} \cdot \nabla)\,\underline{u}$, the divergence form $\mathrm{div}(\underline{u} \otimes \underline{u})$, the skew-symmetric form $\frac{1}{2}(\underline{u} \cdot \nabla)\,\underline{u} + \frac{1}{2}\,\mathrm{div}(\underline{u} \otimes \underline{u})$, and the rotational form $-(\underline{u} \times \mathrm{rot}\,\underline{u}) + \frac{1}{2}\,\nabla\,|\underline{u}|^2$ (here the tensor product of two vectors is expressed by the operator $\otimes$). In the past, the rotational and convective forms were the preferred choices for many flow simulations (see, e.g., Canuto *et al*. [4]), because of their simplicity and computational efficiency. Several authors (e.g., Zang [27] and Blaisdell *et al*. [2]) suggested that, at least for single-domain spectral methods, the skew-symmetric form should be used, in order to minimize aliasing errors. In a recent work, Kravchenko and Moin [18] analyzed aliasing and truncation errors for spectral and finite-difference calculations using different formulations of the nonlinear term. They found that for spectral and higher order finite-difference methods aliasing errors are more harmful than for low-order finite-difference methods. Furthermore, they showed that for Fourier spectral and finite-difference methods the skew-symmetric and the rotational forms are energy conserving even in the presence of aliasing errors. Horiuti and Itami [13] examined the truncation error of the

rotational form for a low-order finite-difference method, which they applied in a direct numerical simulation of turbulent channel flow.

In [25] we showed that the skew-symmetric formulation, as well as the divergence and the standard rotational formulations, of the nonlinear term can lead to numerical instabilities in the staggered $P_N - P_{N-2}$ SEM, while the convective and a variant of the rotational formulation are stable. The purpose of the present paper is to extend this examination to the nonstaggered $P_N - P_{N-2}$ method and to analyze and clarify the observed instabilities. We perform an eigenvalue analysis of the fully discretized system and demonstrate that an instability is introduced by some formulations of the nonlinear term. We show that this instability is not caused by nonlinear effects but that it occurs also for a linearized problem. It is also confirmed that the instability is not affected by the choice of the time-discretization scheme, as it is present already in the semidiscretized equations. Moreover, the influence of the Reynolds number on the instability is discussed.

## 2. DISCRETIZATION OF NAVIER–STOKES EQUATIONS

We consider the incompressible Navier–Stokes equations (NSEs) on a domain $\Omega$ given by

$$\frac{\partial \underline{u}}{\partial t} - \frac{1}{Re}\Delta \underline{u} + \nabla q = -\mathcal{C}(\underline{u})\,\underline{u} + \underline{f}, \tag{1}$$

$$\operatorname{div} \underline{u} = 0, \tag{2}$$

together with appropriate initial and boundary conditions. Here, $\underline{u}$ denotes the velocity, $\mathcal{C}(\underline{u})\,\underline{u}$ is the nonlinear term, $q$ is the pressure, and $\underline{f}$ is a forcing term. The Reynolds number $Re = UL/\nu$ is based on a characteristic velocity $U$, a characteristic length $L$, and the kinematic viscosity $\nu$.

### 2.1. Energy Conservation Properties of Navier–Stokes Equations

The kinetic energy of the flow within $\Omega$ is obtained by multiplying Eq. (1) with $\underline{u}$ and integrating over $\Omega$. This yields

$$\frac{1}{2}\frac{d}{dt}(\underline{u}, \underline{u}) = -\frac{1}{Re}(\nabla \underline{u}, \nabla \underline{u}) + (\underline{f}, \underline{u}) + (q, \operatorname{div} \underline{u}) - (\mathcal{C}(\underline{u})\,\underline{u}, \underline{u}), \tag{3}$$

where, for simplicity, homogeneous Dirichlet boundary conditions for $\underline{u}$ are assumed. The inner product $(\cdot, \cdot)$ is defined by

$$(u, v) = \int_\Omega u(x)v(x)\,dx. \tag{4}$$

Note that the integrals of the pressure gradient and the viscous term are integrated by parts, exploiting the homogeneous boundary conditions. Employing the continuity Eq. (2), the equation of the kinetic energy for a flow without external forces ($\underline{f} = 0$) is given by

$$\frac{1}{2}\frac{d}{dt}(\underline{u}, \underline{u}) = -\frac{1}{Re}(\nabla \underline{u}, \nabla \underline{u}) - (\mathcal{C}(\underline{u})\,\underline{u}, \underline{u}). \tag{5}$$

The convective operator $\mathcal{C}$ is skew-symmetric and conserves kinetic energy, as can be shown easily. Considering the convective term in the form $(\underline{u}\cdot\nabla)\,\underline{u}$, integration by parts for a given vector field $\underline{v}$ yields

$$(\mathcal{C}(\underline{u})\underline{u},\underline{v}) = -(\underline{u},\mathcal{C}(\underline{u})\underline{v}) - (\underline{u}\,\mathrm{div}\,\underline{u},\ \underline{v}) + \int_{\partial\Omega}(\underline{u}\cdot\underline{v})(\underline{u}\cdot\underline{n})\,ds, \tag{6}$$

where $\underline{n}$ is the normal vector on $\partial\Omega$. In the continuous case $\mathrm{div}\,\underline{u}$ vanishes, so that for homogeneous boundary conditions on $\underline{u}$ we obtain

$$(\mathcal{C}(\underline{u})\underline{u},\underline{v}) = -(\underline{u},\mathcal{C}(\underline{u})\,\underline{v}). \tag{7}$$

Thus, the convective operator is skew-symmetric and conserves kinetic energy, since for $\underline{u}=\underline{v}$ Eq. (7) can only be satisfied if

$$(\mathcal{C}(\underline{u})\underline{u},\underline{u}) \equiv 0. \tag{8}$$

In a numerical solution the continuity equation (2) is satisfied only in some discrete sense, with the consequence that $(\underline{u}\,\mathrm{div}\,\underline{u},\underline{u})$ does not vanish exactly in general and the convective operator is not necessarily energy conserving. Whether or not the divergence term $(\underline{u}\,\mathrm{div}\,\underline{u},\underline{u})$ vanishes depends on the discretization of the convective operator.

### 2.2. Spatial Discretization

For the spatial discretization, Eqs. (1) and (2) are transformed into weak form: Find $(\underline{u}, q)$ in $X \times M$ such that $\forall\underline{v}\in X_0$, $\forall g \in M$

$$(\partial\underline{u}/\partial t,\underline{v}) + \frac{1}{Re}(\nabla\underline{u},\nabla\underline{v}) - (q,\mathrm{div}\,\underline{v}) = -(\mathcal{C}(\underline{u})\,\underline{u},\underline{v}) + (\underline{f},\underline{v}), \tag{9}$$

$$(g,\mathrm{div}\,\underline{u}) = 0. \tag{10}$$

The spaces for $\underline{u},\underline{v}$ and $q, g$ are defined as

$$X = \left\{\underline{v}\in\left(\mathcal{H}^1(\Omega)\right)^d,\ \underline{v}\ \text{satisfies the required boundary conditions}\right\}, \tag{11}$$

$$X_0 = \left\{\underline{v}\in\left(\mathcal{H}^1(\Omega)\right)^d,\ \underline{v}=0\ \text{on the boundary}\right\}, \tag{12}$$

$$M = \left\{q\in\mathcal{L}^2(\Omega),\ \int_\Omega q(x)\,dx = 0\right\}, \tag{13}$$

where $d$ is the number of velocity components, $\mathcal{L}^2(\Omega)$ is the space of all square integrable functions over $\Omega$, and $\mathcal{H}^1(\Omega)$ is the space of all functions in $\mathcal{L}^2(\Omega)$ whose first derivatives are also in $\mathcal{L}^2(\Omega)$.

The discretization proceeds by decomposing the computational domain $\Omega$ into a number $K$ of non-overlapping subdomains $\Omega_k$ (spectral elements). In each element the solution is expanded in tensor-product-based polynomials of order $N$, and the discrete polynomial subspaces $X_N \subset X$ and $M_N \subset M$, in which the velocity and the pressure are approximated,

have to be defined properly. For simplicity, in the following we confine ourselves to two-dimensional flows. In order to avoid spurious pressure modes, Maday and Patera [19] suggested the approximation spaces

$$X_{N,0} = X_0 \cap \mathcal{P}^2_{N,K}(\Omega) \times \mathcal{P}^2_{N,K}(\Omega), \tag{14}$$

$$X_N = X \cap \mathcal{P}^2_{N,K}(\Omega) \times \mathcal{P}^2_{N,K}(\Omega), \tag{15}$$

$$M_N = M \cap \mathcal{P}^2_{N-2,K}(\Omega), \tag{16}$$

where $\mathcal{P}_{N,K}$ is the space of all 1D polynomials of degree equal to or less than $N$, restricted to $\Omega_k$, and $\mathcal{P}^2_{N,K}$ is the tensor product of $\mathcal{P}_{N,K}$ in two dimensions. The velocities are approximated by the Lagrange interpolation polynomials based on the $N+1$ Gauss–Lobatto–Legendre (GL) points, and we consider two different approaches for the pressure discretization. The first is the classical staggered method [19], where the pressure is discretized by the Lagrange interpolation polynomials based on the $N-1$ Gauss–Legendre (G) points. The second approach is the nonstaggered method (see, e.g., [22]), where the pressure is discretized at the $N-1$ inner GL points in each spectral element. In both cases we refer to the respective set of points as "pressure points." For the nonstaggered approach all inner products in (9) and (10) are evaluated by Gauss–Lobatto integration. In the staggered method the terms $(q, \operatorname{div} \underline{v})$ and $(g, \operatorname{div} \underline{u})$ are evaluated by Gauss integration, while all other terms are evaluated by Gauss-Lobatto integration. Note that all higher dimensional integration rules are obtained by tensor products of the 1D formulas.

The final discretized weak form of Eqs. (1) and (2) then reads: Find $(\underline{u}, q) \in X_N \times M_N$ such that $\forall \underline{v} \in X_{N,0}$ and $\forall g \in M_N$

$$(\partial \underline{u}/\partial t, \underline{v})_N + \frac{1}{Re}(\nabla \underline{u}, \nabla \underline{v})_N - (q, \operatorname{div} \underline{v})_N = -(\mathcal{C}(\underline{u})\,\underline{u}, \underline{v})_N + (\underline{f}, \underline{v})_N, \tag{17}$$

$$(g, \operatorname{div} \underline{u})_N = 0, \tag{18}$$

where $(\cdot, \cdot)_N$ indicates the discrete inner product. Since the velocity $\underline{u}$ and the test functions $\underline{v}$ are defined in spaces different from those of the pressure $q$ and the test functions $g$, interpolations have to be used before the integrals in $(q, \operatorname{div} \underline{v})_N$ and $(g, \operatorname{div} \underline{u})_N$ can be evaluated.

As pointed out before, the nonlinear term can be written in different ways. The various formulations analyzed in the present paper are summarized in Table I. Note that all derivatives of $\underline{u}$ are computed at the velocity points. This is in contrast to the continuity equation (18), where the derivatives of $\underline{u}$ are computed at the pressure points.

**TABLE I**
**Formulations of the Convective Term**

| Notation | $C(\underline{u})\,\underline{u}$ | Description | S/U |
|---|---|---|---|
| $C_{conv}(\underline{u})\,\underline{u}$ | $(\underline{u} \cdot \nabla)\,\underline{u}$ | Convective form | S |
| $C_{div}(\underline{u})\,\underline{u}$ | $\operatorname{div}(\underline{u} \otimes \underline{u})$ | Divergence form | U |
| $C_{skew}(\underline{u})\,\underline{u}$ | $\frac{1}{2}(\underline{u} \cdot \nabla)\,\underline{u} + \frac{1}{2}\operatorname{div}(\underline{u} \otimes \underline{u})$ | Skew-symmetric form | U |

*Note.* $\underline{u} \otimes \underline{v}$ is the tensor product of $\underline{u}$ and $\underline{v}$. The inner product is $\underline{u} \cdot \underline{v}$; $\underline{u}$ is the velocity. $S$ = stable, $U$ = unstable, according to present analysis.

### 2.3. Temporal Discretization

The semidiscrete Eqs. (17) and (18) are now discretized in time, assuming $\underline{f} \equiv 0$. The linear terms $1/Re\,(\nabla \underline{u}, \nabla \underline{v})_N$ and $(q, \operatorname{div} \underline{v})_N$ are treated implicitly, while the nonlinear term $(\mathcal{C}(\underline{u})\,\underline{u}, \underline{v})_N$ is treated explicitly. Two different time-discretization schemes are employed. The first scheme we use is a Crank–Nicolson scheme for the linear term and the pressure, together with a third-order Adams–Bashforth method (CN/AB3) for the nonlinear term. The second scheme employs a third-order backward differentiation scheme for the linear term together with a third-order extrapolation for the nonlinear term (BDF3/EX3), according to Karniadakis *et al.* [15]. The latter is discussed in the following in more detail.

The BDF3/EX3 time discretization leads to a fully discretized form of the NSEs

$$\left[\frac{1}{Re}\underline{\underline{E}} + \kappa \underline{\underline{B}}\right] \underline{u}^{n+1} - \underline{\underline{D}}^T q^{n+1} = \frac{1}{\Delta t}\left[3\underline{\underline{B}}\,\underline{u}^n - \frac{3}{2}\underline{\underline{B}}\,\underline{u}^{n-1} + \frac{1}{3}\underline{\underline{B}}\,\underline{u}^{n-2}\right] + 3\underline{\underline{C}}(\underline{u}^n)\,\underline{u}^n - 3\underline{\underline{C}}(\underline{u}^{n-1})\,\underline{u}^{n-1} + \underline{\underline{C}}(\underline{u}^{n-2})\,\underline{u}^{n-2}, \tag{19}$$

$$\underline{\underline{D}}\,\underline{u}^{n+1} = 0, \tag{20}$$

where $\underline{\underline{E}}, \underline{\underline{D}}^T, \underline{\underline{D}}$, and $\underline{\underline{C}}$ denote the discrete versions of the Laplacian, the gradient, the divergence, and convective operators, respectively. $\underline{\underline{B}}$ is the (diagonal) mass matrix with $\kappa = 11/(6\Delta t)$. Herein $\underline{u}^n$ and $q^n$ denote the pointwise values of $\underline{u}$ and $q$ at velocity and pressure points, respectively, at time step $t^n = n\,\Delta t$. The fully discrete system (19), (20) can be recast into the general form

$$\begin{bmatrix} \underline{\underline{H}} & -\underline{\underline{D}}^T \\ -\underline{\underline{D}} & 0 \end{bmatrix} \begin{bmatrix} \underline{u}^{n+1} \\ q^{n+1} \end{bmatrix} = \begin{bmatrix} \underline{g} \\ 0 \end{bmatrix}, \tag{21}$$

with the Helmholtz operator

$$\underline{\underline{H}} = \left[\frac{1}{Re}\underline{\underline{E}} + \kappa \underline{\underline{B}}\right],$$

and where the right-hand side has the form

$$\underline{g} = \underline{g}\,(\underline{\underline{C}}(\underline{u}^n)\,\underline{u}^n, \underline{\underline{C}}(\underline{u}^{n-1})\,\underline{u}^{n-1}, \underline{\underline{C}}(\underline{u}^{n-2})\,\underline{u}^{n-2}, \underline{u}^n, \underline{u}^{n-1}, \underline{u}^{n-2}).$$

The general form (21) can be solved using the classical Uzawa algorithm (see, e.g., [3]). In this approach the momentum equation is formally solved for the velocity $\underline{u}^{n+1}$, which is then inserted into the continuity equation. This leads to an equation for the pressure,

$$\underbrace{\underline{\underline{D}}\,\underline{\underline{H}}^{-1}\,\underline{\underline{D}}^T}_{=:\underline{\underline{S}}}\, q^{n+1} = -\underline{\underline{D}}\,\underline{\underline{H}}^{-1}\,\underline{g} =: \underline{r}_q, \tag{22}$$

with the right-hand side $\underline{r}_q$. From the pressure $q^{n+1}$ the velocity $\underline{u}^{n+1}$ is evaluated according to Eq. (21).

Beside the Uzawa algorithm we also employed a special time-splitting approach for the $P_N - P_{N-2}$ SEM suggested by Maday *et al.* [20] and extended to more general finite-element methods by Perot [21]. This approach, which was used for example by Couzy [6] and Fischer [8], is similar to the Uzawa algorithm in that no pressure boundary conditions

are needed. However, since we obtained essentially the same instability results as for the Uzawa algorithm, we confine our presentation to the latter algorithm. (Note that the time-splitting approach in [20] is not to be confused with the classical time-splitting method [5, 15] often used in $P_N - P_N$ SEMs).

## 3. RESULTS

### 3.1. Numerical Results for the Different Formulations

The classical $P_N - P_{N-2}$ SEM, in which velocity is discretized at the GL points and pressure at the G points, was applied previously to various flow problems. Maday and Patera [19], in their fundamental paper on this technique, simulated the 2D flow past a cylinder at $Re = 150$ and the flow around a cylinder in a grooved channel at $Re = 225$. Couzy [6] performed a simulation of the flow over a backward-facing step in 3D at Reynolds numbers up to $Re = 343$. Only very few simulations using this $P_N - P_{N-2}$ SEM at significantly higher Reynolds numbers have been presented so far, one of these being the study of 2D flow past a cylinder at $Re = 9500$ by Fischer [8]. He also reported on the simulation of the linear-stability problem of plane channel flow at $Re = 7500$, where the parabolic mean flow is disturbed by small-amplitude 2D Tollmien–Schlichting waves. The growth rate of the perturbation energy was compared with the solution from linear-stability theory and it was shown that for sufficiently fine discretization an excellent agreement is achieved. The same test case was studied in our previous work [25], where we showed that good agreement with the linear-stability theory can only be obtained if the convective form of the nonlinear term is employed. The divergence form or the skew-symmetric form, on the other hand, led to numerical instabilities. Note that in [8] Fischer also used the convective form (private communication, 1999). The present method was employed in [26] for a study of the 3D forward-facing step flow.

#### 3.1.1. *Nonlinear Results and Linearization*

The numerical instabilities observed in [25] are analyzed more closely in the following. As a test case we consider a 2D plane channel flow at $Re = 7500$, based on half channel height and centerline velocity, with periodic boundary conditions in the streamwise direction and no-slip conditions at the walls. The flow is driven by a pressure gradient $dP/dx = -2/Re$. As an initial condition, a laminar Poiseuille profile is prescribed, which is disturbed by numerical noise of order $10^{-12}$. We computed the time history of the perturbation energy

$$E(t) = \int_0^{2\pi} \int_{-1}^{1} \left[ \left(1 - x_2^2 - u_1\right)^2 + u_2^2 \right] dx_1\, dx_2 \tag{23}$$

obtained for different formulations of the nonlinear term according to Table I. In Fig. 1 the results for the classical staggered approach are shown. It is evident from the figure that the simulation results are strongly dependent on the formulation of the nonlinear term. For the divergence form and the skew-symmetric form $E(t)$ grows exponentially and the simulation becomes unstable. A stable solution is obtained for the convective form only. In Fig. 2 the simulation results for the nonstaggered $P_N - P_{N-2}$ SEM are shown. It is remarkable that we obtain the same stability behavior as for the classical approach (i.e., the divergence and skew-symmetric forms are unstable and the convective form is stable).

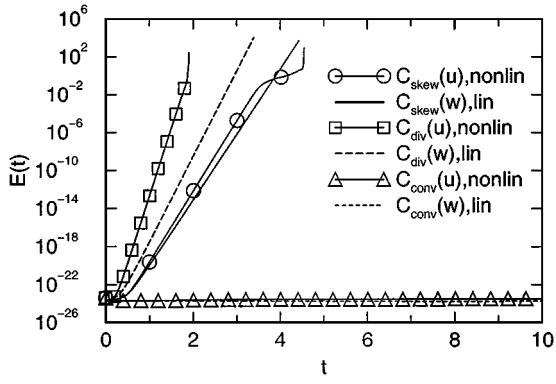


**FIG. 1.** Time history of perturbation energy $E(t)$ in plane channel flow for classical staggered $P_N - P_{N-2}$ SEM. Comparison of results from Navier–Stokes simulations (nonlin) and simulations based on the Oseen equations (lin). Results for different formulations of the convective term $C$ ($Re = 7500$, $4 \times 4$ elements, $N = 8$).

To simplify the problem and exclude nonlinear effects, we consider the Oseen equations [1] which are the linearized form of the NSEs

$$\frac{\partial \underline{u}}{\partial t} - \frac{1}{Re}\Delta \underline{u} + \nabla q = -\mathcal{C}(\underline{w})\underline{u}, \tag{24}$$

$$\operatorname{div} \underline{u} = 0, \tag{25}$$

where $\underline{w}$ is a given divergence-free velocity field. At this point we confine our presentation of the linear results to the classical (staggered) approach. For our test case, $\underline{w}$ is taken as the laminar plane Poiseuille flow. The results obtained for different formulations of the linearized convective operator are also given in Fig. 1. It can be seen that for the linearized divergence and skew-symmetric forms the amplification rate of the perturbation energy is smaller than for the nonlinear case, but the energy nonetheless also grows exponentially (for $E(t) < 10^{-2}$). It is evident from the figure that a linear numerical instability is introduced by the divergence form and the skew-symmetric form of the convective term, which is not related to nonlinear effects.

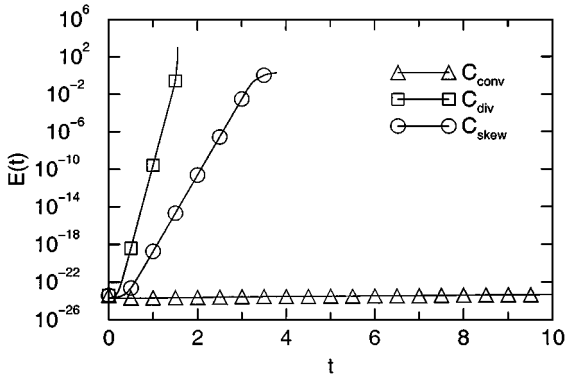


**FIG. 2.** Time history of perturbation energy $E(t)$ in plane channel flow for nonstaggered $P_N - P_{N-2}$ SEM. Navier–Stokes simulation for different formulations of the convective term $C$ ($Re = 7500$, $4 \times 4$ elements, $N = 8$).

We analyzed this instability with respect to its dependence on the temporal and spatial resolution and found no effect on the general stability properties. (Of course, the time step was always chosen well below the CFL stability limits of the EX3 and AB3 schemes, respectively.) Furthermore, the effect of the boundary conditions was tested. In SEM only $C^0$ continuity over the boundaries is required, which means that the derivatives of the velocity are not forced to be periodic. In order to exclude the possibility that the stability problem originates from the special treatment of the periodic boundaries, we conducted simulations where the periodic boundary conditions were replaced by Dirichlet conditions, and encountered the same instability. *Only for sufficiently low Reynolds numbers* (*below* $Re = 100$, *in the considered problem*) *did all the schemes remain stable, irrespective of the treatment of the nonlinear terms*. This is obviously due to viscous damping, as discussed in the following. We remark here that the formulation $C_{conv}$ remains stable far beyond the short initial time shown in Fig. 1. We have conducted simulations over long integration times, $t > 1000$, in which this formulation did not develop any instability.

### 3.1.2. *Effect of Viscous Damping*

It is interesting to note that we found the skew-symmetric form to be unstable, while other investigations (e.g., Rønquist [23], who used the nonstagger $P_N - P_{N-2}$ SEM) suggested that it should be the preferred choice in $P_N - P_{N-2}$ SEM. However, Rønquist [23] analyzed a plane channel flow at the rather low Reynolds number of about 200, while we consider a test case for $Re = 7500$, where the physical damping is much smaller. Although for low Reynolds numbers the numerical instability is masked by the physical damping, accuracy suffers from this ("unstable") formulation of the nonlinear term. To investigate the influence of the skew-symmetric form on accuracy, we employed the staggered SEM to the simulation of the Orr–Sommerfeld test problem, used by Fischer [8], but for lower Reynolds numbers. In Fig. 3 we compare the exact solution of the linear stability theory with the simulation results at $Re = 100$ and $Re = 500$. For $Re = 500$, where viscous damping is already very small, the simulation becomes unstable. On the other hand, the simulation for $Re = 100$ remains stable, but the damping rate does not agree with the exact rate for $Re = 100$; it rather

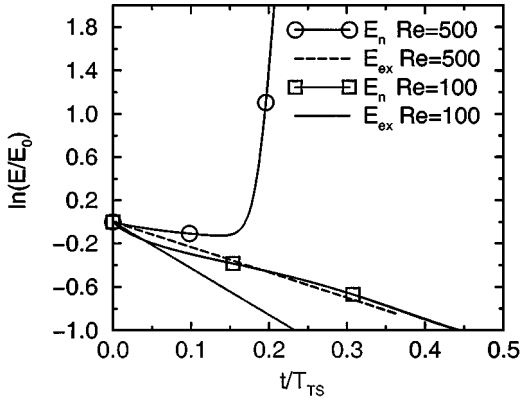


**FIG. 3.** Time history of computed perturbation energy $E_n$ in plane channel flow for convective operator in skew-symmetric form at different Reynolds numbers ($N = 12$, $2 \times 2$ elements). Comparison with results $E_{ex}$ of linear stability theory. (Results for staggered method.)

agrees with that for $Re = 500$. *Thus, even for low Reynolds numbers where the scheme is stable, inaccurate growth rates are obtained when using the skew-symmetric form.*

### 3.2. Discussion of the Discretized Convective Term

3.2.1. *Nonlinear Operators*

Since numerical instability is related to the formulation of the nonlinear term, it is appropriate to investigate the discretized nonlinear term. In the continuous case all formulations of $\mathcal{C}$ are equivalent and the divergence form can be transformed into the convective form by means of the continuity equation

$$\mathcal{C}(\underline{u})\underline{u} = \operatorname{div}(\underline{u} \otimes \underline{u}) = (\underline{u} \cdot \operatorname{grad})\,\underline{u} + \underline{u} \underbrace{\operatorname{div} \underline{u}}_{=0}. \tag{26}$$

However, in the discrete case the divergence form is numerically equivalent to the convective form *plus* an additional divergence term, i.e.

$$(C_{div}(\underline{u})\underline{u}, \underline{v})_N \equiv (\operatorname{div}(\underline{u} \otimes \underline{u}), \underline{v})_N = ((\underline{u} \cdot \operatorname{grad})\,\underline{u}, \underline{v})_N + \underbrace{(\underline{u} \operatorname{div} \underline{u}, \underline{v})_N}_{\neq 0}. \tag{27}$$

The divergence term on the right-hand side of Eq. (27) does not vanish exactly, because the continuity constraint is enforced at the pressure points only.

Note that in the computation of the products in the nonlinear term, Eq. (27), and in similar equations later in this work, additional aliasing errors occur. A possible concern is that these aliasing errors could cause the observed instability. In fact, for a Fourier spectral scheme Kravchenko and Moin [18] reported that the instability that occurred with some formulations of the nonlinear term could be removed by dealiasing. However, P. F. Fischer (private communication, 2001) found that for the same numerical scheme as used herein (i.e., $P_N - P_{N-2}$ SEM based on a staggered grid) dealiasing did not remove the instability. Note also that aliasing errors can be made very small by increasing the resolution, whereas the divergence term will turn out to be dominant and to cause the observed instabilities, which become worse with increasing resolution. For this reasons, aliasing errors are not explicitly considered in the present paper.

For a further investigation of the divergence term, we consider an abridged operator consisting of the second term of Eq. (27) only,

$$(C_a(\underline{u})\underline{u}, \underline{v})_N := (\underline{u} \operatorname{div} \underline{u}, \underline{v})_N. \tag{28}$$

For a plane parallel flow such as the undisturbed plane Poiseuille flow the first term in Eq. (26) vanishes, so that $C_a$ is equal to $C_{div}$ of Eq. (27). Performing an (undisturbed) Poiseuille flow simulation with this form of the convective operator, we found that the $L_2$-norm of the divergence at the pressure points indeed remains at roundoff-error level, while the divergence of $\underline{u}$ at the velocity points grows exponentially in time. In Fig. 4 and Fig. 5 results are shown for the staggered and nonstaggered $P_N - P_{N-2}$ SEM, respectively. After $t = 2.5$ the divergence at the pressure points increases also and the simulation blows up, due to nonlinear effects. Furthermore, it is obvious from Fig. 4 and Fig. 5 that the growth of the divergence at the velocity points, $\|\operatorname{div}_{GL,u}\|$, is related to the growth of the perturbation

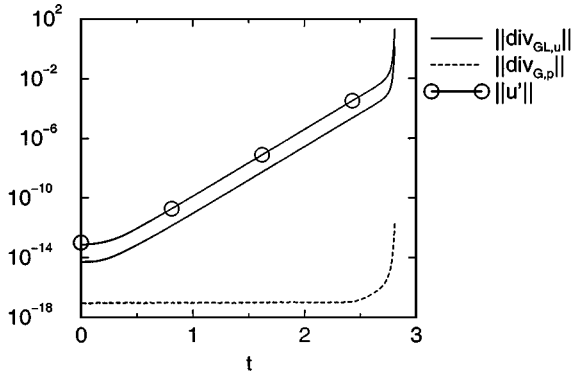


**FIG. 4.** Results for staggered $P_N - P_{N-2}$ SEM. Comparison of divergence error in $L_2$-norm at pressure points $\|\mathrm{div}_{G,p}\|$ and at velocity points $\|\mathrm{div}_{GL,u}\|$, and the perturbation velocity $\|\underline{u}'\|$, for the abridged convective operator $C_a(\underline{u})$.

velocity $\|\underline{u}'\| := \|(u_1 - (1 - x_2^2), u_2)^T\|$, which has the same slope but is about two orders of magnitude larger than $\|\mathrm{div}_{GL,u}\|$.

Further numerical simulation results show that the operator

$$(\mathrm{div}\,(\underline{u} \otimes \underline{u}), \underline{v})_N - (\underline{u}\,\mathrm{div}\,\underline{u}, \underline{v})_N, \tag{29}$$

which is equivalent to the convective form $(C_{conv}(\underline{u})\underline{u}, \underline{v})_N$, is stable, while the operator

$$((\underline{u} \cdot \mathrm{grad})\underline{u}, \underline{v})_N + (\underline{u}\,\mathrm{div}\,\underline{u}, \underline{v})_N, \tag{30}$$

which is equivalent to the divergence form $(C_{div}(\underline{u})\underline{u}, \underline{v})_N$, is unstable. This clearly demonstrates that it is indeed the term $C_a$ of Eq. (28) which causes the instability. For the same reason, the skew-symmetric form is unstable, as it is equivalent to

$$C_{conv} + \frac{1}{2} C_a. \tag{31}$$

It can be concluded that *in the $P_N - P_{N-2}$ SEM, although the numerical scheme enforces the continuity constraint pointwise at the pressure points, it still may let the divergence*

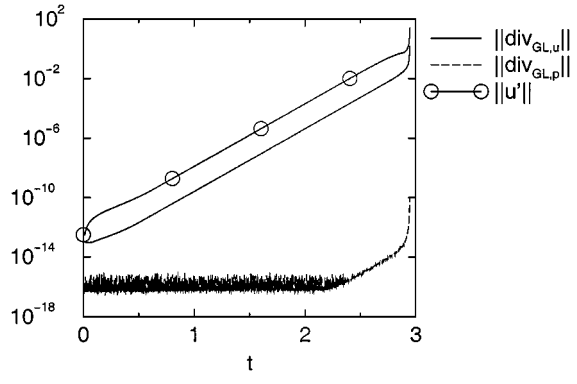


**FIG. 5.** Results for nonstaggered $P_N - P_{N-2}$ SEM. Comparison of divergence error in $L_2$-norm at pressure points $\|\mathrm{div}_{GL,p}\|$ and velocity points $\|\mathrm{div}_{GL,u}\|$, and the perturbation velocity $\|\underline{u}'\|$, for the abridged convective operator $C_a(\underline{u})$.

*error grow exponentially at certain velocity points* (*i.e., those which differ from the pressure points*), *allowing numerical instabilities to develop.*

### 3.2.2. *Linearized Model for the Convective Operator*

In Section 3.1.1 we presented numerical results for the Oseen problem, and in particular we showed that the simulation becomes unstable for the linearized skew-symmetric and divergence forms. Thus, the instability is even present in the linearized NSE. In this section we discuss the relation between nonlinear and linearized convective operators.

For the example of a slightly disturbed plane Poiseuille flow the numerical solution $\underline{u}$, which fulfills the continuity equation only in a weak sense at the pressure points (see Eq. (18)), can be decomposed into a given divergence-free velocity $\underline{w} = (1 - x_2^2, 0)^T$ and an "error term" $\underline{\varepsilon}$, i.e.

$$\underline{u} = \underline{w} + \underline{\varepsilon}. \tag{32}$$

With this decomposition the divergence form can be written, in the discrete sense, as

$$\begin{aligned}(\mathrm{div}(\underline{u} \otimes \underline{u}), \underline{v})_N &= (\mathrm{div}(\underline{u} \otimes (\underline{w} + \underline{\varepsilon})), \underline{v})_N \\ &= (\mathrm{div}(\underline{u} \otimes \underline{w}), \underline{v})_N + (\mathrm{div}(\underline{u} \otimes \underline{\varepsilon}), \underline{v})_N \end{aligned} \tag{33}$$

or as

$$\begin{aligned}(\mathrm{div}(\underline{u} \otimes \underline{u}), \underline{v})_N &= (\mathrm{div}((\underline{w} + \underline{\varepsilon}) \otimes \underline{u}), \underline{v})_N \\ &= (\mathrm{div}(\underline{w} \otimes \underline{u}), \underline{v})_N + (\mathrm{div}(\underline{\varepsilon} \otimes \underline{u}), \underline{v})_N. \end{aligned} \tag{34}$$

Using $\underline{w}$ there are two different ways to linearize the convection operator in divergence form, namely $\mathrm{div}(\underline{u} \otimes \underline{w})$ and $\mathrm{div}(\underline{w} \otimes \underline{u})$. The two linearizations are not equal for $\underline{\varepsilon} \neq 0$ (note that the second terms on the right-hand side of Eqs. (33) and (34) differ). The two linearized forms can be transformed into

$$(\mathrm{div}(\underline{u} \otimes \underline{w}), \underline{v})_N = \underbrace{(\underline{u}\,\mathrm{div}\,\underline{w}, \underline{v})_N}_{=0} + \underbrace{((\underline{w} \cdot \nabla)\,\underline{u}, \underline{v})_N}_{C_{conv}} \tag{35}$$

and analogously

$$(\mathrm{div}(\underline{w} \otimes \underline{u}), \underline{v})_N = \underbrace{(\underline{w}\,\mathrm{div}\,\underline{u}, \underline{v})_N}_{\neq 0} + ((\underline{u} \cdot \nabla)\underline{w}, \underline{v})_N. \tag{36}$$

For the first linearization (35) the divergence form is equal to the (linearized) convective form and is hence stable. In contrast, the linearization in (36) exhibits the same instability behavior as the fully nonlinear operator, which is evident from Fig. 1. Linearizations analogous to Eq. (36) are performed also for the convective and the skew-symmetric forms and they are summarized in Table II.

We denote the matrices corresponding to the linearized convective operators of Table II by $\underline{\underline{C}}_{conv}$, $\underline{\underline{C}}_{div}$, and $\underline{\underline{C}}_{skew}$. In Fig. 6 the eigenvalues of the matrices $\underline{\underline{C}}_{conv}$, $\underline{\underline{C}}_{div}$, and $\underline{\underline{C}}_{skew}$ are shown. It is seen that for $\underline{\underline{C}}_{conv}$ all eigenvalues lie on the imaginary axis. Furthermore,

**TABLE II**
**Linearized Convective Operators**

| Notation | $C(\underline{w})\,\underline{u}$ | Description |
|---|---|---|
| $C_{conv}(\underline{w})\,\underline{u}$ | $(\underline{w}\cdot\nabla)\,\underline{u}$ | Linearized convective form |
| $C_{div}(\underline{w})\,\underline{u}$ | $\mathrm{div}\,(\underline{w}\otimes\underline{u})$ | Linearized divergence form |
| $C_{skew}(\underline{w})\,\underline{u}$ | $\frac{1}{2}(\underline{w}\cdot\nabla)\,\underline{u}+\frac{1}{2}\mathrm{div}(\underline{w}\otimes\underline{u})$ | Linearized skew-symmetric form |

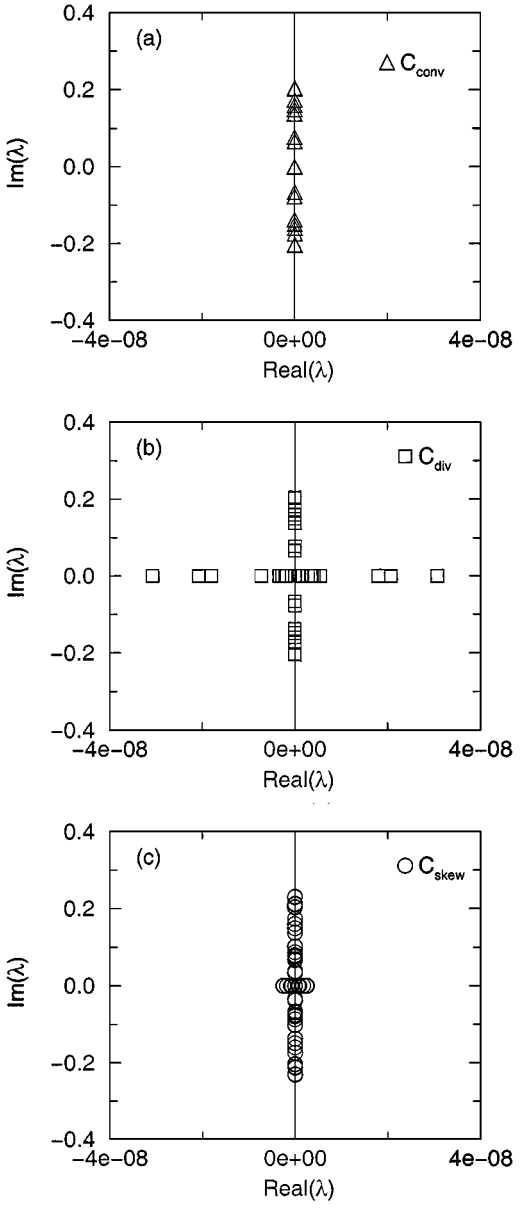


**FIG. 6.** Eigenvalues of the matrix $\underline{\underline{C}}$. (a) Convective form, (b) divergence form, and (c) skew-symmetric form, for $N = 4$, $2 \times 2$ elements.

the operator is skew-symmetric up to machine accuracy, and thus energy conserving (see Section 2.1). For $\underline{\underline{C}}_{div}$ and $\underline{\underline{C}}_{skew}$, on the other hand, we found eigenvalues with positive real parts which are small ($\sim 10^{-9} - 10^{-8}$), but significantly larger than roundoff-error level. Among other things this shows that in the present case *the discretized skew-symmetric form is in fact not skew-symmetric*. We computed the error in the skew-symmetry and it was of the same order as the real parts of the eigenvalues shown in Fig. 6.

### 3.3. Eigenvalue Analysis of the Fully Discretized Linear System

We have shown in the previous section that some of the linearized convection operators have positive eigenvalues, suggesting numerical instabilities. However, to assess the stability properties of the discretized NSEs we have to consider the eigenvalues of the fully (temporally and spatially) discretized system. For simplicity, we confine our presentation to a time discretization with the explicit Euler scheme for the nonlinear terms and the implicit Euler scheme for the linear terms here. However, we have analyzed the higher order methods BDF3/EX3, Eq. (19), and CN/AB3 as well. As explained previously, the general form (21) is decoupled by the Uzawa algorithm, which leads to the equation for the pressure (22) in which the right-hand-side $\underline{r}_q$ contains the nonlinear and linear terms at time-step $t^n$. Solving this pressure equation and substituting the pressure back into the velocity equation yields a complicated matrix relation of the form

$$\underline{u}^{n+1} = [(\underline{\underline{H}}^{-1}\underline{\underline{D}}^T\underline{\underline{S}}^{-1}\underline{\underline{D}} + \underline{\underline{I}})\underline{\underline{H}}^{-1}] \cdot [\underline{\underline{C}}(\underline{w}) + \underline{\underline{L}}]\underline{u}^n, \tag{37}$$

for which we introduce the abbreviation

$$\underline{u}^{n+1} =: \underline{\underline{A}}\,\underline{u}^n, \tag{38}$$

where $\underline{\underline{S}}$ is the pressure matrix defined in Eq. (22) and $\underline{\underline{L}}$ represents the linear terms. It should be noted that the boundary conditions are incorporated into the discrete operators. $\underline{\underline{A}}$ is the discrete time evolution operator, which has to be analyzed for stability as follows. An approximation of the derivative $\partial\underline{u}/\partial t$ at $t^n$ is given by

$$\frac{\partial \underline{u}}{\partial t} \approx \frac{\underline{u}^{n+1} - \underline{u}^n}{\Delta t} = \underline{\underline{F}}\,\underline{u}^n, \tag{39}$$

where by Eq. (38)

$$\underline{\underline{F}} := \frac{1}{\Delta t}(\underline{\underline{A}} - \underline{\underline{I}}). \tag{40}$$

Due to consistency, $\underline{\underline{F}}$ is practically independent of the time-step $\Delta t$ if $\Delta t$ is chosen sufficiently small. The condition for a stable integration of nongrowing solutions is that the real parts $\lambda_j^r$ of all eigenvalues of $\underline{\underline{F}}$ are less than or equal to zero (cf. Hirsch [12]), i.e.

$$\lambda_j^r \le 0, \quad \forall j. \tag{41}$$

#### 3.3.1. *Numerical Results*

We first show the results for the classical staggered $P_N - P_{N-2}$ method. In Fig. 7 the eigenvalues of $\underline{\underline{F}}$ are given for $\underline{\underline{C}}_{conv}$, $\underline{\underline{C}}_{div}$, and $\underline{\underline{C}}_{skew}$ in Eq. (37) ($N = 4$, $2 \times 2$ elements).

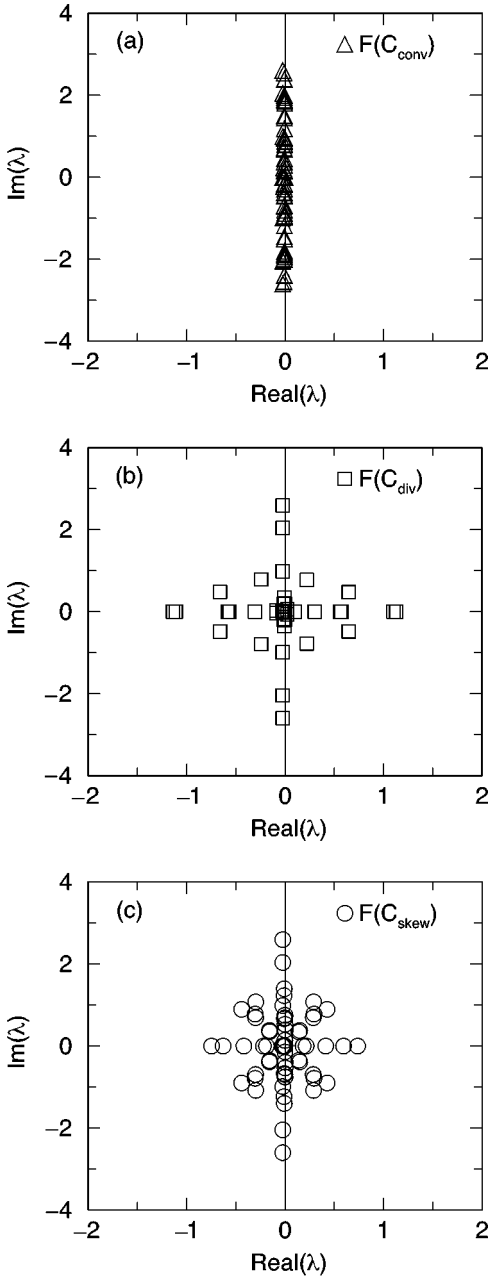


**FIG. 7.** Results for staggered $P_N - P_{N-2}$ SEM. Eigenvalues of the matrix $\underline{\underline{F}}$ of the fully discretized system. (a) Convective form, (b) divergence form, and (c) skew-symmetric form, for $N = 4$, $2 \times 2$ elements.

The numerical data (see Table III and Table IV) clearly show that for the convective form the real parts of the eigenvalues are negative ($\max(\lambda_j^r) =: \lambda_{max}^r \approx -3.3 \times 10^{-4}$), while they are positive for the divergence form ($\lambda_{max}^r \approx 1.13$) and the skew-symmetric form ($\lambda_{max}^r \approx 0.736$). Thus, condition (41) is violated for the divergence form and the skew-symmetric form, which leads to the numerical instability observed. Furthermore, in Fig. 8 the same eigenvalue behavior can be seen for the nonstaggered $P_N - P_{N-2}$ SEM. For

**TABLE III**
**Eigenvalues of the Fully Discretized System**

| $N$ | $\underline{\underline{F}}(\underline{\underline{C}}_{conv})$ | $\underline{\underline{F}}(\underline{\underline{C}}_{skew})$ | $\underline{\underline{F}}(\underline{\underline{C}}_{div})$ |
|---|---|---|---|
| 2 | −3.2747E − 4 | 0.0799 | 0.3542 |
| 4 | −3.2899E − 4 | 0.7363 | 1.1287 |
| 6 | −3.2899E − 4 | 2.1817 | 3.0082 |
| 8 | −3.2899E − 4 | 4.0854 | 5.2528 |
| 10 | −3.2899E − 4 | 6.3289 | 7.6979 |
| 12 | −3.2899E − 4 | 8.8198 | 10.216 |
| 14 | −3.2899E − 4 | 11.498 | 12.707 |

*Note.* Maximal real parts of the eigenvalues of the fully discretized system ($\lambda^r_{max}$ of matrix $\underline{\underline{F}}$), for different convective operators, as a function of the polynomial degree $N$ on the elements. $Re = 7500$, $\Delta t = 10^{-4}$, $2 \times 2$ elements. (Results for staggered method.)

the convective form the real parts of the eigenvalues are also negative (and of the same magnitude as in Fig. 7(a)), while significant positive real parts are found for the divergence and skew-symmetric forms. Moreover, it can be seen from Fig. 9 that for the unstable formulation $\underline{\underline{C}}_{div}$ (for the staggered approach) the eigenvalue with maximal real part $\lambda^r_{max}$ grows with the polynomial degree $N$, and that the real part of the eigenvalue is positive even for the smallest possible polynomial degree (i.e., for $N = 2$).

In addition to this examination of the implicit/explicit Euler method, we confirmed the same instability for the BDF3/EX3 and CN/AB3 time-discretization schemes with practically identical eigenvalues $\lambda^r_{max}$ of the corresponding matrices $\underline{\underline{F}}$. The instability was also present when the Uzawa algorithm was replaced by a time-splitting scheme [20] applied to the $P_N - P_{N-2}$ method.

It should be noted that the largest positive eigenvalue $\lambda^r_{max}$ indeed agrees with one half of the observed amplification rate of the kinetic energy for the various linearized formulations of the convective term, as it should. For example (for the staggered method), with $N = 8$ and $4 \times 4$ elements, $\lambda^r_{max} \approx 10.42$ for the divergence form and $\lambda^r_{max} \approx 8.03$ for the skew-symmetric form, while the corresponding slopes in Fig. 1 (in the linear region $0.7 \leq t \leq 1.3$) are about 20.5 and 15.5 for the divergence and skew-symmetric forms, respectively.

**TABLE IV**
**Eigenvalues of the Fully Discretized System**

| $K_1 \times K_2$ | $2 \times 2$ | $2 \times 4$ | $4 \times 4$ |
|---|---|---|---|
| $\underline{\underline{F}}(\underline{\underline{C}}_{conv})$ | −3.2899E − 4 | −3.2899E − 4 | −3.2899E − 4 |
| $\underline{\underline{F}}(\underline{\underline{C}}_{skew})$ | 4.0854 | 5.23592 | 8.0334 |
| $\underline{\underline{F}}(\underline{\underline{C}}_{div})$ | 5.2528 | 6.45622 | 10.4224 |

*Note.* $\lambda^r_{max}$ of matrix $\underline{\underline{F}}$, for different convective operators, as a function of the number of elements. $N = 8$, $\Delta t = 10^{-4}$, $Re = 7500$. (Results for staggered method.)

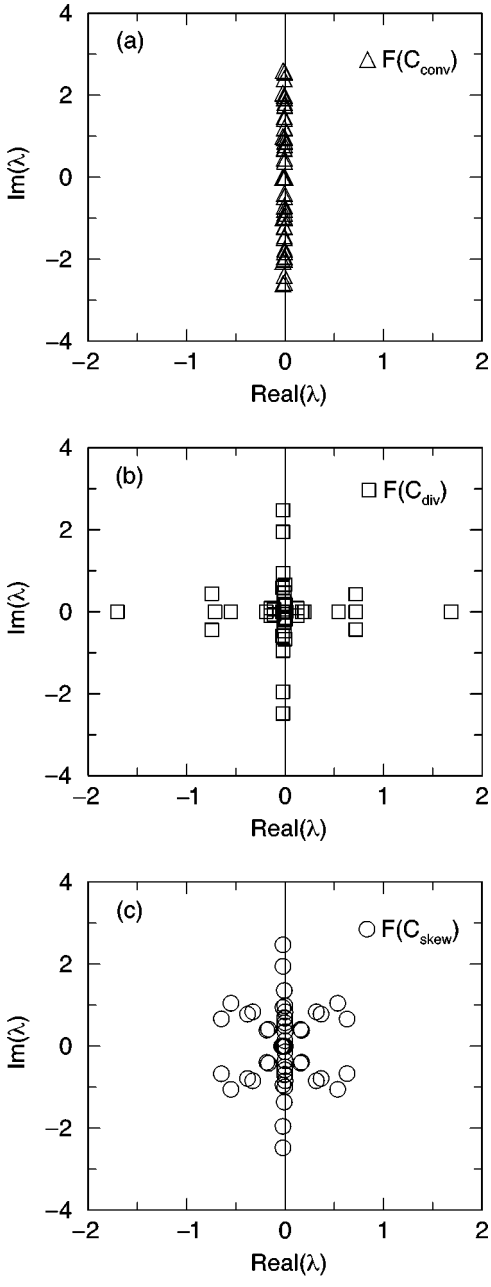


**FIG. 8.** Results for nonstaggered $P_N - P_{N-2}$ SEM. Eigenvalues of the matrix $\underline{\underline{F}}$ of the fully discretized system. (a) Convective form, (b) divergence form, and (c) skew-symmetric form, for $N = 4$, $2 \times 2$ elements.

### 3.3.2. *Reynolds Number Influence*

We investigated the influence of the Reynolds number *Re* on the stability behavior, using again plane Poiseuille flow as a test problem. In Fig. 10 and Table V the maximum of the real parts of the eigenvalues are given as a function of *Re* for different formulations of $\underline{\underline{C}}$ (for the staggered method). It can be seen that for the divergence and the skew-symmetric forms

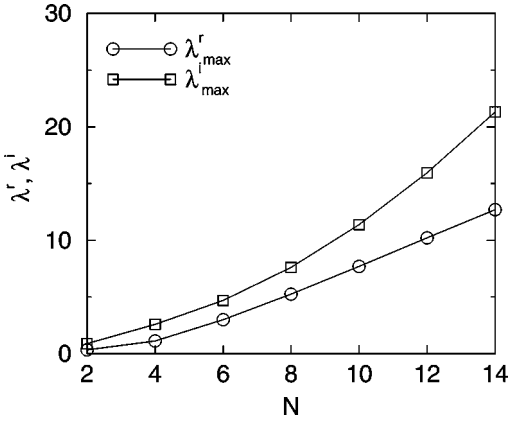


**FIG. 9.** Maximum real parts and imaginary parts of eigenvalues of matrix $\underline{\underline{F}}$ for $\underline{\underline{C}}_{div}$, as a function of the polynomial degree $N$. (Results for staggered $P_N - P_{N-2}$ SEM.)

$\lambda^r_{max}$ becomes positive at $Re \approx 40$ and $Re \approx 100$, respectively, while for the convective form $\lambda^r_{max}$ remains negative for all Reynolds numbers. In Fig. 10 and Fig. 11 a log–log plot of $|\lambda^r_{max}|$ is shown as a function of $Re$ for the staggered and nonstaggered approaches, respectively. It is obvious from the curves that for low Reynolds numbers $\lambda^r_{max}$ grows

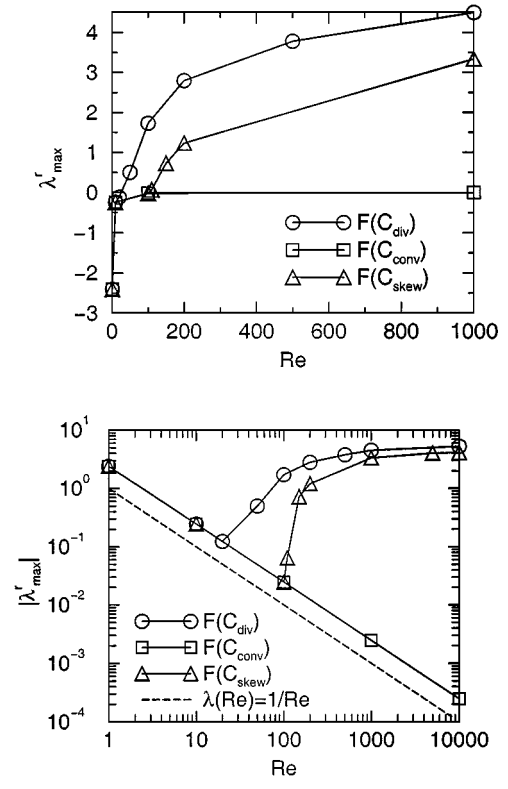


**FIG. 10.** Maximum real eigenvalues of matrix $\underline{\underline{F}}$ of the fully discretized system, for different formulations of $\underline{\underline{C}}$ as a function of the Reynolds number $Re$ ($2 \times 2$ elements, $N = 8$). Linear and logarithmic representation of $\lambda^r_{max}$ and $|\lambda^r_{max}|$, respectively. (Results for staggered $P_N - P_{N-2}$ SEM.)

**TABLE V**
**Eigenvalues of the Fully Discretized System**

| *Re* | 10 | 40 | 100 | 1000 | 7500 | 10000 |
|---|---|---|---|---|---|---|
| $\underline{\underline{F}}(\underline{\underline{C}}_{conv})$ | −0.2461 | −6.1685E − 2 | −2.4667E − 2 | −2.4673E − 3 | −3.2899E − 4 | −2.4673E − 4 |
| $\underline{\underline{F}}(\underline{\underline{C}}_{skew})$ | −0.2461 | −0.0617 | 0.0246 | 3.3368 | 4.0854 | 4.1121 |
| $\underline{\underline{F}}(\underline{\underline{C}}_{div})$ | −0.2461 | 0.0664 | 1.7254 | 4.4962 | 5.2528 | 5.2782 |

*Note.* $\lambda^r_{max}$ of matrix $\underline{\underline{F}}$ for different convective operators, as a function of *Re*. $N = 8$, $\Delta t = 10^{-4}$, $2 \times 2$ elements. (Results for staggered method.)

proportionally to $1/Re$ for all three formulations, which is identical to the results obtained for a Fourier discretization scheme. However, for higher Reynolds numbers $\lambda^r_{max}$ grows much faster (and finally becomes positive) for the divergence and skew-symmetric forms. Thus, for low-enough Reynolds numbers all three formulations are stable, which agrees with the results of Rønquist [23], who found the skew-symmetric form to be stable for $Re \leq 100$ for the same test problem. However, we recall that the computed time evolution nevertheless is likely to be inaccurate for the unstable formulations, as was demonstrated by example of Fig. 3.

## 4. SUMMARY AND DISCUSSION

In this study we investigated the effects of the formulation of the nonlinear term on the numerical stability of certain spectral element methods. We have shown that, in the framework of $P_N - P_{N-2}$ spectral element simulations of the time-dependent NSEs, only the convective form is stable, while the divergence and skew-symmetric forms are unstable. A numerical eigenvalue analysis revealed that this instability is caused by the spatial discretization in the latter forms. We have analyzed both the classical staggered [19] and the nonstaggered [22] $P_N - P_{N-2}$ SEMs and obtained the same stability behavior for the two methods.

The numerical instability is related to the divergence error of the computed solution at those velocity points where the continuity equation is not enforced by the numerical

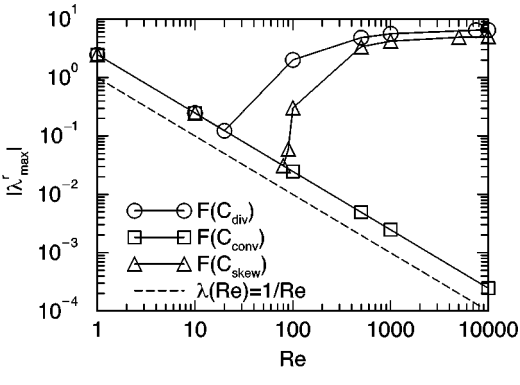


**FIG. 11.** Results for nonstaggered $P_N - P_{N-2}$ SEM. Maximum real eigenvalues of matrix $\underline{\underline{F}}$ of the fully discretized system, for different formulations of $\underline{\underline{C}}$ as a function of the Reynolds number *Re* ($2 \times 2$ elements, $N = 8$) in logarithmic representation.

scheme. We have also shown that the discretized skew-symmetric form $C_{skew}$ is not exactly skew-symmetric. Thus, the skew-symmetric form does not conserve kinetic energy, which may finally lead to a numerical instability.

This observed stability behavior is in contrast to the situation with Fourier methods, where the skew-symmetric form is found to be stable [18, 27]. Moreover, in [18] aliasing errors are shown to be lower with the skew-symmetric form than with the convective and divergence forms. Also, aliasing errors are reduced with increasing resolution, while for the unstable formulation using the $P_N - P_{N-2}$ SEM, the instability growth rate increases with the resolution. Here the divergence error is much more severe than aliasing errors, which are generally present as well.

The instability is present in all time-discretization schemes, and it is independent of temporal resolution. In fact, the instability is introduced by the spatial-discretization scheme already in the semidiscretized equations. Only viscous damping at sufficiently low Reynolds numbers can stabilize the scheme. For very low Reynolds numbers ($Re < 40$, in the example considered) all formulations are stable, but it is shown that for low Reynolds numbers the skew-symmetric form gives inaccurate temporal predictions.

## ACKNOWLEDGMENTS

We appreciate helpful discussions with M. O. Deville, P. F. Fischer, C. Härtel, and M. Melenk. We are grateful to N. Adams for comments on a draft version of this paper. We also thank the referees for their constructive criticism.

## REFERENCES

1. G. K. Batchelor, *An Introduction to Fluid Dynamics* (Cambridge Univ. Press, Cambridge, UK, 1990).
2. G. A. Blaisdell, E. T. Spyropoulos, and J. H. Qin, The effect of the formulation of nonlinear terms on aliasing errors in spectral methods, *Appl. Numer. Math.* **21**, 207 (1996).
3. F. Brezzi and M. Fortin, *Mixed and Hybrid Finite Element Methods* (Springer-Verlag, New York/Berlin, 1991).
4. C. Canuto, M. Y. Hussaini, A. Quarteroni, and T. A. Zang, *Spectral Methods in Fluid Dynamics* (Springer-Verlag, Heidelberg, 1988).
5. A. J. Chorin, Numerical solution of the Navier–Stokes equations, *Math. Comput.* **22**, 745 (1968).
6. W. Couzy, *Spectral Element Discretization of the Unsteady Navier–Stokes Equations and its Iterative Solution on Parallel Computers*, Thèsis No. 1380 (École Polytechnique Fédéral de Lausanne, 1995).
7. W. Couzy and M. O. Deville, A fast Schur complement method for the spectral element discretization of the incompressible Navier–Stokes equations, *J. Comput. Phys.* **116**, 135 (1995).
8. P. F. Fischer, An overlapping Schwarz method for spectral element solution of the incompressible Navier–Stokes equations, *J. Comput. Phys.* **133**, 84 (1997).
9. P. M. Gresho, Incompressible fluid dynamics: Some fundamental formulation issues, *Annu. Rev. Fluid Mech.* **23**, 413 (1991).
10. C. Härtel, Turbulent flows: Direct numerical simulation and large-eddy simulation, in *Handbook of Computational Fluid Mechanics*, edited by R. Peyret (Academic, New York, 1996), p. 283.
11. C. Härtel, L. Kleiser, M. Michaud, and C. F. Stein, A direct numerical simulation approach to the study of intrusion fronts, *J. Eng. Math.* **32**, 103 (1997).
12. C. Hirsch, *Numerical Computation of Internal and External Flows Vol. 1* (Wiley, Chichester, 1989).
13. K. Horiuti and T. Itami, Truncation error analysis of the rotational form for the convection terms in Navier–Stokes equation, *J. Comput. Phys.* **145**, 671 (1998).
14. G. E. Karniadakis and R. D. Henderson, Spectral element methods for incompressible flows, in *The Handbook of Fluid Dynamics*, edited by R. W. Johnson (CRC Press, Boston, 1998), p. 29-1.

15. G. E. Karniadakis, M. Israeli, and S. A. Orszag, High-order splitting methods for incompressible Navier–Stokes equations, *J. Comput. Phys.* **97**, 414 (1991).
16. L. Kleiser and U. Schumann, Treatment of the incompressibility and boundary conditions in 3-D numerical spectral simulation of plane channel flows, in *Proceedings of the 3rd GAMM Conference on Numerical Methods in Fluid Mechanics*, edited by E. H. Hirschel (Vieweg, Braunschweig, 1980), p. 165.
17. L. Kleiser, C. Härtel, and T. Wintergerste, There is no error in the Kleiser–Schumann influence matrix method, *J. Comput. Phys.* **141**, 85 (1998).
18. A. G. Kravchenko and P. Moin, On the effects of numerical errors in large eddy simulations of turbulent flows, *J. Comput. Phys.* **131**, 310 (1997).
19. Y. Maday and A. T. Patera, Spectral element methods for the incompressible Navier–Stokes equations, in *State-of-the-Art-Surveys in Computational Mechanics*, edited by A. K. Noor (ASME, New York, 1989), p. 71.
20. Y. Maday, A. T. Patera, and E. M. Rønquist, An operator-integration-factor splitting method for time-dependent problems: Application to incompressible fluid flow, *J. Sci. Comput.* **5**, 263 (1990).
21. J. B. Perot, An analysis of the fractional step method, *J. Comput. Phys.* **108**, 51 (1993).
22. E. M. Rønquist, A domain decomposition solver for the steady Navier–Stokes equation, in *Proceedings of the 3rd International Conference on Spectral and Higher Order Methods*, edited by A. V. Ilin and L. R. Scott (Houston Journal of Mathematics, Houston, 1996), p. 469.
23. E. M. Rønquist, Convection treatment using spectral elements of different order, *Int. J. Numer. Methods Fluids* **22**, 241 (1996).
24. S. J. Sherwin and G. E. Karniadakis, Tetrahedral *hp* finite elements: Algorithms and flow simulations, *J. Comput. Phys.* **124**, 14 (1996).
25. D. Wilhelm and L. Kleiser, Stable and unstable formulations of the convection operator in spectral element simulations, *Appl. Numer. Math.* **33**, 275 (2000).
26. D. Wilhelm, *Numerical Investigation of Three-Dimensional Separation in a Forward-Facing Step Flow Using a Spectral Element Method*, Thesis No. 13774 (Eidgenössische Technische Hochschule Zürich), in Reihe 7, 404, VDI-Verlag, Düsseldorf, 2001.
27. T. A. Zang, On the rotation and skew-symmetric forms for incompressible flow simulations, *Appl. Numer. Math.* **7**, 27 (1991).